Observation of Vacancy Defect Migration in the Cation Sublattice of Complex Oxides by ^{18}O Tracer Experiments

René Meyer and Rainer Waser
Institut für Werkstoffe der Elektrotechnik, RWTH Aachen, Germany

Julia Helmbold and Günter Borchardt
Institut für Metallurgie, TU Clausthal, Germany
(Received 21 August 2002; published 12 March 2003)

We report on ^{18}O tracer diffusion experiments and model calculations for the study of cation vacancy migration in oxide crystals. The model takes advantage of the electrostatic coupling forces between anion and cation defects that allow the evolution of the cation vacancy profile to be observed by anion tracer experiments. Applied to $SrTiO_3$, the ambipolar diffusion of strontium vacancies with $H_A = 3.5$ eV was found to be the dominant reequilibration mechanism of the cation sublattice. This result is in contrast to earlier studies proposing the formation of SrO intergrowth phases.

DOI: 10.1103/PhysRevLett.90.105901 PACS numbers: 66.30.Hs, 61.72.Ji

Ternary perovskite-type oxides (ABO_3) show either insulating, semiconducting, mixed electronic-ionic conducting, or, at lowest temperatures, superconducting behavior. The respective electrical property of the material is determined, at a given temperature, oxygen activity, and thermal pretreatment, by the impurity dopant type and level and, more decisively, by intrinsic self-doping with donor-type oxygen vacancies and acceptor-type cation vacancies. Oxygen vacancy formation and migration in perovskites, and also in other oxides, has been the subject of numerous investigations [1–7]. It is well known that, at moderate temperatures, the concentration of anion lattice defects is correlated with the oxygen partial pressure pO_2 via point defect reactions. The defect reaction [8] of oxygen vacancies ($V_O^{\cdot\cdot}$), electrons (e'), and regular oxygen sites ($O_O^{\times}$) is given by

$$1/2\ O_2(g) + 2e' + V_O^{\cdot\cdot} \overset{\text{ox}}{\rightarrow} O_O^{\times}. \quad (1)$$

The kinetics of transition of the anion sublattice is limited by oxygen vacancy migration [6]. At lower temperatures, the surface reaction (1) becomes the rate-limiting step [2]. Cation nonstoichiometry, which is predominant, e.g., in donor-doped perovskites, has not yet been studied in detail. Nonetheless, metal vacancies, formed at high temperatures, are considered to play a key role in the bulk conductivity of donor-doped and undoped oxides as well as in the establishment of resistive grain boundaries [9]. Hence, a detailed understanding of the nature of cation vacancy formation and migration is of broad scientific and technological interest.

For the model material $SrTiO_3$, Schottky-type defects are assumed to form in the cation sublattice by an *internal* defect reaction [10,11]. The defect reaction of regular metal ions ($Sr_{Sr}^{\times}$) and regular oxygen ions reads as

$$O_O^{\times} + Sr_{Sr}^{\times} \overset{\text{ox}}{\rightarrow} V_{Sr}'' + V_O^{\cdot\cdot} + SrO_{\text{RP phase}}. \quad (2)$$

Accompanied by the formation of oxygen vacancies ($V_O^{\cdot\cdot}$) and strontium vacancies (V_{Sr}''), Eq. (2) predicts the establishment of rocksalt intergrowth layers [Ruddlesden-Popper (RP) phases [12], $AO \cdot (ABO_3)_n$] inside the material. The kinetics of transition may be *reaction controlled*. Experimental proof of an RP phase formation according to Eq. (2) has not been given as yet. Instead, recent studies indicate an alternative defect mechanism, where strontium vacancies or the SrO-rich second phase can be exclusively created at the surface of single crystals (s.c.) [13]. Then, the reequilibration kinetics is limited by cation *diffusion*. The point defect reaction of the cation sublattice may then be written as follows:

$$1/2\ O_2(g) + 2e' + Sr_{Sr}^{\times} \overset{\text{ox}}{\rightarrow} V_{Sr}'' + SrO_{\text{second phase}}. \quad (3)$$

This Letter presents a method consisting of ^{18}O tracer

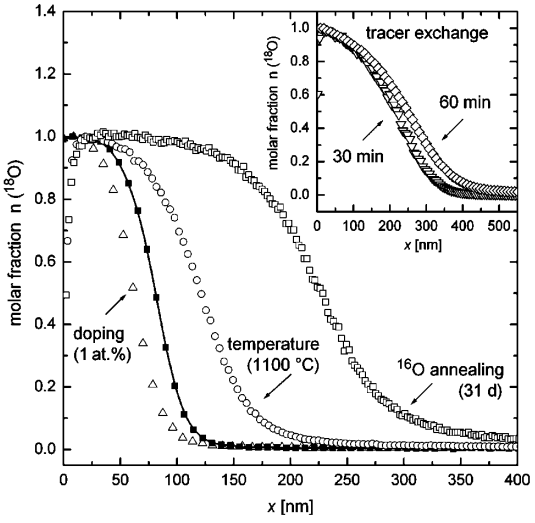

FIG. 1. ^{18}O tracer diffusion profiles. Filled squares: Characteristic shape of the tracer profile obtained for $T_{dwell} = 1050\,°C$, $\tau_{an} = 5$ d, $\tau_{ex} = 30$ min, 0.2 at. % Nb. Open symbols: Influence of T_{dwell}, oxygen annealing time τ_{an}, amount of dopant N_D, and tracer exchange time τ_{ex} (inset).

experiments and model calculations for studying the reequilibration mechanism of the metal sublattice in view of diffusion or reaction control. In contrast to common ^{18}O tracer experiments, where a uniform distribution of oxygen vacancies is essential to evaluate the tracer diffusion coefficient, this method takes advantage of the spatial distribution of oxygen vacancies that evolves in strong correlation with cation vacancy defects. The experimental part is based on a detailed parameter study of ^{18}O tracer diffusion in donor-doped $SrTiO_3$. Since $SrTiO_3$ serves as model material, the method can be generalized to perovskite-type or other oxidic compounds.

The procedure consists of a preannealing in $^{16}O_2$ followed by an isotope exchange in $^{18}O_2$. First, reduced (as-grown) (100)-oriented single crystals (Crystec, Germany) with optical surface finish were oxidized in air for an annealing period τ_{an}. Subsequently, the tracer experiment was performed under constant thermodynamic conditions (temperature, pO_2) for different exchange times, $\tau_{ex} \ll \tau_{an}$ being chosen to ensure that no significant shift of defect concentrations in the crystal occurs during the exchange. In addition, temperature T_{dwell} and doping level N_D were varied. Tracer profiles were investigated by SIMS (VG Simslab) using an Ar^+ primary beam of 7.5 keV. Only ^{32}O, ^{34}O, and ^{36}O were detected by a quadrupole mass spectrometer to avoid a saturation of the secondary ion detection system. The molar fraction of oxygen $n(^{18}O)$ was calculated from the dimer intensities $I(32)$, $I(34)$, and $I(36)$. Sputtered crater depths were determined by a profilometer.

Figure 1 illustrates the tracer profiles obtained. Instead of the expected classical error-function shape, all curves reveal three regions. In the near-surface region, a pronounced plateau is found. It is followed by an S-shaped drop of the ^{18}O concentration. In some experiments region three shows a linear tail. This behavior, which could be associated with fast diffusion paths along extended defects, like subgrain boundaries, will be neglected in the discussion. The curve marked by filled squares represents the typical tracer profile; curves depicted with open symbols indicate the dependence on each experimental parameter. The penetration depth of the tracer profile increases strongly with τ_{an} and T_{dwell}. Surprisingly, the diffusion length decreases significantly with an increasing amount of doping, whereas only a weak influence of τ_{ex} was found.

In the analysis, both oxidation and tracer experiments were simulated by numerical calculations. The underlying model is based on the *a priori* hypothesis of a random diffusion of all ionic and electronic defects (V''_{Sr}, $V^{\cdot\cdot}_O$, e'). A sketch of the proposed mechanism is shown in Fig. 2(b). The decisive role of strontium vacancies is supported by the results of our previous work [13], where a SrO_x secondary phase as shown in Fig. 2(a) was found at the surfaces of oxidized La-doped and Nb-doped single crystals. Here the influence of temperature, amount

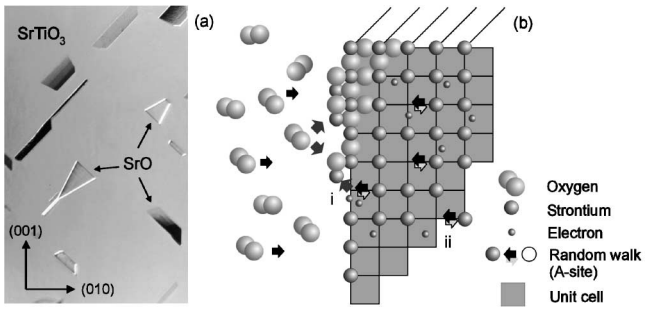

FIG. 2. (a) SrO precipitates formed at the surface of 1 at.% La-doped $SrTiO_3$ s.c. after oxygen annealing at 1300 °C. (b) Proposed reequilibration mechanism of the cation sublattice: Increasing oxygen activity surface forces a fast formation of SrO at the crystal surface (i). Strontium vacancies remaining in the cation sublattice slowly diffuse into the crystal (ii).

of doping, and annealing time strongly suggest a slow indiffusion of cation vacancies as the rate-limiting process in the equilibration kinetics. The formation of RP phases was also studied by high resolution TEM. Since no evidence for a formation of this defect type was found [14], this mechanism is excluded in the present model.

Choosing a continuous medium approach, particle flux densities j_i of electrons, strontium vacancies, and oxygen vacancies are given by

$$j_i = -D_i \frac{dC_i}{dx} + \frac{z_i}{|z_i|} \mu_i C_i E, \qquad i \in \{V^{\cdot\cdot}_O, V''_{Sr}, e'\}, \quad (4)$$

where D_i denotes the self-diffusion coefficient, C_i the particle concentration, μ_i ($= |z_i| q_0 D_i / k_B T$, Nernst-Einstein relation) the mobility, z_i the charge number, and E the electric field inside the material, which is calculated by the integral over the local space charge ρ in each slice of the crystal. Applying Maxwell's first equation and the material equation, we obtain E for a donor content N_D:

$$\rho(x) = q_0 \sum_k z_k C_k(x), \qquad k \in \{V^{\cdot\cdot}_O, V''_{Sr}, e', N^{\cdot}_D\}, \quad (5)$$

$$E(x) = \frac{1}{\varepsilon} \int_0^x \rho(\xi) d\xi, \quad (6)$$

where q_0 denotes the elementary charge and ε is the low-frequency permittivity. The field dependence of ε was neglected for simplicity. The electric field originates from local space charges created by a shift in the centers of charge of mobile majority defects. In the studied system, it couples the diffusion of majority defects (e', V''_{Sr}) and minority defects ($V^{\cdot\cdot}_O$). Hence, the diffusion of strontium vacancies leaves a "footprint" in the oxygen sublattice that can be experimentally observed by the ^{18}O tracer. Boundary conditions for oxygen vacancies and strontium vacancies were derived from Eqs. (1) and (3). Hereby, both surface reactions were assumed to be fast. The surface concentration of electrons was calculated

from the global electroneutrality condition. The following discussion will treat the case of oxidation in agreement with the experimental procedure. According to Eqs. (1) and (3), a high oxygen activity will cause an increase of strontium vacancies at the surface, while the concentration of electrons and oxygen vacancies will decrease. Using a finite differences method, the evolution of the defect profiles and the electric field was calculated by solving the convection-diffusion Eq. (4) for all mobile species. Material constants, self-diffusion coefficients of electrons and oxygen vacancies, and mass action coefficients were taken from the related literature [6,11,15].

The self-diffusion coefficient of the cation vacancies was determined by fitting model simulations to experimental data (see next section). Results are shown in Fig. 3. Arrows denote the evolution of the concentrations and of the internal electric field. As expected, strontium vacancies diffuse into the bulk and electrons migrate towards the surface. A negative internal electric field is formed by local space charges that accelerates the ionic and slows down the electronic species. A minority flux of oxygen vacancies also occurs, revealing an unexpected result. After a fast drop of the concentration in the whole crystal (not shown), an enrichment of oxygen vacancies against the concentration gradient is observed (''uphill diffusion''). It is ascribed to the negative internal field that drives the positively charged anion vacancies towards the surface. As shown in Fig. 3, the local variation of the oxygen vacancy concentration is found to be very sensitive to the reequilibration process in the cation and the electronic sublattice. In the following, we will elucidate the influence of an oxygen vacancy enrichment situated in the near-surface region on the shape of the ^{18}O tracer depth profile. Equation (7) links the tracer diffusion coefficient D_O^{Tr} and the oxygen vacancy concentration [16]:

$$D_O^{Tr}(x) = f \times \frac{[V_O^{\cdot\cdot}](x)}{[O_O^{\times}]} D_{V_O}^{self}, \qquad f = 0.68. \tag{7}$$

Here f denotes the correlation factor for tracer diffusion in cubic lattices and $D_{V_O}^{self}$ represents the self-diffusion coefficient of oxygen vacancies.

Figure 4 shows the tracer diffusion coefficient versus penetration depth calculated from Eq. (7). Because of the enrichment of oxygen vacancies, the highest diffusion coefficient is located at the surface. For a calculation of the temporal and spatial evolution of the ^{18}O profile from the tracer diffusion coefficient, we combined Fick's law and the continuity equation:

$$\frac{\partial[^{18}O]}{\partial t} = D_O^{Tr} \times \frac{\partial^2[^{18}O]}{\partial x^2} + \frac{\partial D_O^{Tr}}{\partial x} \times \frac{\partial[^{18}O]}{\partial x}. \tag{8}$$

Here $[^{18}O]$ denotes the oxygen tracer concentration. According to the simulation results in Fig. 4, the tracer profile can be reproduced in all details. The field-induced enrichment of oxygen vacancies at the surface is regarded as the key feature of the model. It yields a tracer diffusion coefficient that exceeds the bulk value by up to 5 orders of magnitude and leads to the nonconventional S-shape regime in the tracer profile due to a marked decrease in the tracer diffusion coefficient.

A variation of the cation vacancy self-diffusion coefficient in our model even permits quantitative agreement to be achieved. With respect to the variation of all experimental parameters, we found excellent agreement between model predictions and experimental data by the use of a temperature-dependent cation self-diffusion coefficient. This contribution focuses on the temperature dependence. The dependence on other parameters will

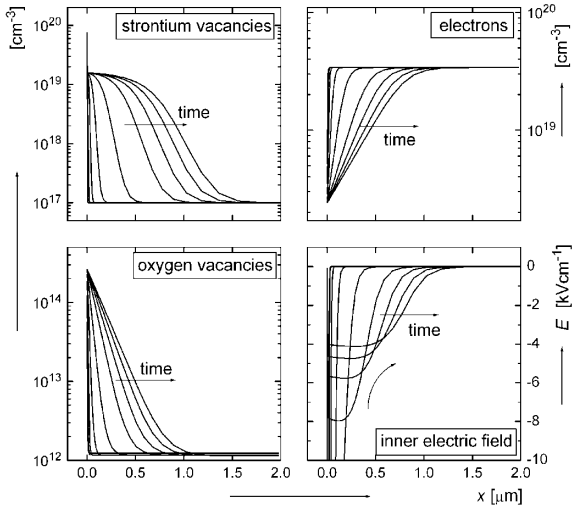

FIG. 3. Simulated concentration profiles for strontium vacancies, electrons, oxygen vacancies as well as the spatial variation of the internal electric field during oxidation of $SrTiO_3$ (parameter: elapsed time). The negative field is mainly created by the Coulomb interaction between electrons and strontium vacancies (ambipolar diffusion).

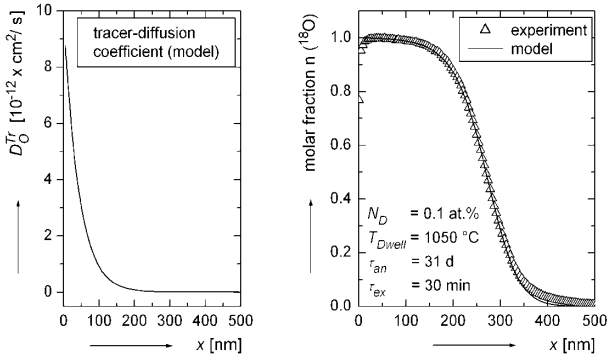

FIG. 4. Spatial variation of the ^{18}O tracer diffusion coefficient calculated from the oxygen vacancy profile taken from Fig. 3 (left). The proposed model explains the characteristic evolution of the tracer profile, which originates from the high tracer diffusion coefficient in the near-surface region and the low diffusion coefficient in the interior of the crystal (right).

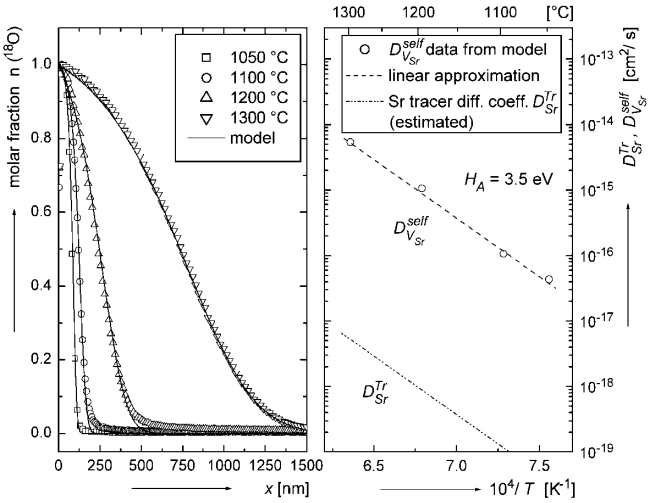

FIG. 5. (Left) Experiments (symbols) and model calculations (lines) of ^{18}O tracer profiles as a function of temperature for 0.2 at. % Nb-doped $SrTiO_3$. The strontium vacancy self-diffusion coefficient $D^{self}_{V_{Sr}}$ was varied for best match. (Right) Arrhenius plot of $D^{self}_{V_{Sr}}$ and $D^{Tr}_{Sr} \approx D^{self}_{V_{Sr}} \times [V''_{Sr}]/[Sr^{\times}_{Sr}]$.

be reported in detail in a forthcoming paper. Figure 5 illustrates experimental data and simulations covering the studied temperature range between 1050 °C and 1300 °C. Self-diffusion coefficients of strontium vacancies $D^{self}_{V_{Sr}}$ were determined by comparing numerical data with experimental curves. For a dopant content of about 0.2 at. %, $D^{self}_{V_{Sr}}(T)$ reveals an Arrhenius behavior:

$$D^{self}_{V_{Sr}}(T) = 10^{-3} \exp\left(-\frac{3.5\ \text{eV}}{k_B T}\right)\left[\frac{\text{cm}^2}{\text{s}}\right]. \qquad (9)$$

For higher dopant concentrations, a weak tendency of $D^{self}_{V_{Sr}}$ to increase was observed. The activation enthalpy of 3.5 eV found in our study is higher than the value of 2.5 eV obtained from *ab initio* calculations [17]. A value of 2.8 eV was determined for 1.1 at. % Nb-doped (SrCa)TiO_3 ceramics using an impedance spectroscopy technique to study the oxidation of grain boundaries [18]. Concerning a Schottky-type reaction inside the crystal by a formation of RP phases, we were not able to explain the shape of the tracer profile nor its dependence on the experimental parameters. Hence, we concluded that the diffusion of cation vacancies from the surface into the bulk is the dominant reequilibration mechanism and the rate-limiting step in the equilibration process studied.

In summary, we report here on a new method for studying cation vacancy diffusion by ^{18}O tracer experiments. The underlying idea is to take advantage of the electrostatic forces between charged defects in the different crystal sublattices, which allows the evolution of cation vacancies by oxygen vacancies to be observed. Applied to donor-doped $SrTiO_3$, the oxidation of reduced single crystals was found to be governed by the outward diffusion of strontium, i.e., the inward diffusion of strontium vacancies, and not by the formation of RP phases. A quantitative determination of the strontium vacancy self-diffusion coefficient as a function of temperature was carried out by matching experimental data with model calculations. We regard this combination of experiment and model simulations to be a potential method for improving fundamental knowledge on cation vacancy formation and migration in similar material systems where tracer mobility is too low (see, e.g., Fig. 5) to perform conventional cation tracer studies.

We are indebted to S. Weber for the SIMS analysis. Financial support by the Deutsche Forschungsgemeinschaft (DFG) made this work possible.

[1] A. E. Paladino, L. G. Rubin, and J. S. Waugh, J. Phys. Chem. Solids **26**, 391–397 (1965).
[2] J. Claus, M. Leonhardt, and J. Maier, J. Phys. Chem. Solids **61**, 1199–1207 (2000).
[3] N. H. Chan, R. K. Sharma, and D. M. Smyth, J. Electrochem. Soc. **128**, 1762–1769 (1981).
[4] J. G. Bednorz and K. A. Müller, Rev. Mod. Phys. **60**, 585–600 (1988).
[5] C. Tragut and K. H. Härdtl, Sens. Actuators B, Chem. **4**, 425–429 (1991).
[6] R. Waser, T. Baiatu, and K. H. Härdtl, J. Am. Ceram. Soc. **73**, 1645–1673 (1990).
[7] R. Waser, T. Bieger, and J. Maier, Solid State Commun. **76**, 1077–1081 (1990).
[8] For defect notations used, see F. A. Kröger and H. J. Vink, Solid State Phys. **3**, 307 (1956).
[9] J. Daniels and R. Wernicke, Philips Res. Rep. **31**, 544–559 (1976).
[10] U. Balachandran and N. G. Eror, J. Electrochem. Soc. **129**, 1021–1026 (1982).
[11] R. Moos and K. H. Härdtl, J. Am. Ceram. Soc. **80**, 2549–2562 (1997).
[12] S. N. Ruddlesden and P. Popper, Acta Crystallogr. **11**, 54–55 (1958).
[13] R. Meyer, R. Waser, J. Helmbold, and G. Borchardt, J. Electroceram. **9**, 103–112 (2002).
[14] C. Jia (private communication).
[15] K. H. Hellwege and A. M Hellwege, in *Oxide*, Landolt-Börnstein, Gruppe III, Band 16a (Springer-Verlag, Berlin, Heidelberg, New York, 1981).
[16] J. Philibert, *Atom Movements* (Les Éditions de Physique, Les Ulis, France, 1991).
[17] M. J. Akhtar *et al.*, J. Am. Ceram. Soc. **78**, 421–428 (1995).
[18] F. Poignant, Ph.D. thesis, Université de Limoges, E.N.S.C.I., France, 1995.